

# Transduction Mechanisms of the Fabry-Perot Polymer Film Sensing Concept for Wideband Ultrasound Detection

Paul C. Beard, Frédéric Pérennès, and Tim N. Mills

**Abstract**—The transduction mechanisms of a wideband (30 MHz) contact ultrasound sensor based upon the use of a thin polymer film acting as a Fabry-Perot interferometer have been investigated. Polyethylene terephthalate (PET) sensing elements, illuminated by the free-space collimated output of a wavelength-tunable DBR laser diode, have been used to study the sensor transfer function, sensitivity, the effect of water absorption, and frequency response characteristics. Acoustic performance was evaluated by comparing the sensor output with that of a calibrated PVDF membrane hydrophone using laser-generated acoustic transients as a source of broadband ultrasound. An ultrasonic acoustic phase sensitivity of 0.1 rad/MPa, a linear operating range to 5 MPa, and a noise-equivalent-pressure of 20 kPa over a 25 MHz measurement bandwidth were obtained using a water-backed 50  $\mu\text{m}$  PET sensing film. A model of frequency response that incorporates the effect of an adhesive layer between the sensor film and backing material has been developed and validated for different sensing film thicknesses, backing configurations, and adhesive layer thicknesses.

## I. INTRODUCTION

THIS paper describes the operating principles of a wideband ultrasound transducer based upon the interferometric detection of acoustically-induced changes in the optical thickness of a thin polymer film acting as a Fabry-Perot sensing interferometer. The concept has been previously demonstrated in a variety of probe-type configurations in which the polymer film sensing element is mounted at the tip of an optical fiber [1]. These include a miniature ultrasonic optical fiber hydrophone [2]–[4] and a photoacoustic probe [5]. The use of an optical fiber can, however, introduce a number of complicating factors that degrade the sensitivity and frequency response of the sensor. For example, the fringe visibility of the interferometer, and therefore its sensitivity, is reduced when illuminated by the divergent output of a multimode optical fiber [6]. The extent and uniformity of the sensor frequency response also can be significantly degraded due to acoustic diffraction

Manuscript received April 30, 1999; accepted July 20, 1999. This work was carried out in collaboration with Precision Acoustics Ltd., UK, and funded under the EPSRC/DTI LINK Photonics Programme.

P. C. Beard and T. N. Mills are with the Department of Medical Physics and Bioengineering, University College London, London WC1E 6JA, UK (e-mail: p.beard@medphys.ucl.ac.uk).

F. Pérennès is with Synchrotrone Trieste, in Area Science Park, 34012 Trieste, Italy.

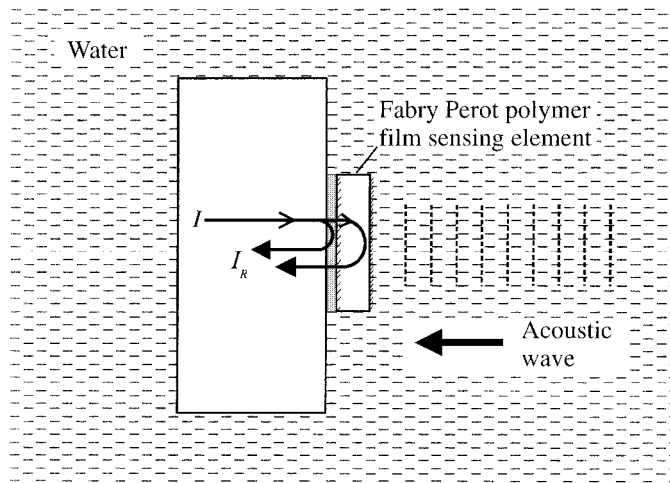


Fig. 1. Schematic of sensing configuration.

around the fiber-tip and the finite thickness of the adhesive layer used to bond the polymer film sensing element to the fiber. In order to study the underlying transduction mechanisms, it is desirable to avoid these effects, or at least make them easier to control. This can be achieved by dispensing with the optical fiber and illuminating the sensing element with a free space collimated laser beam. The use of such an approach forms the subject of this paper. Specifically, the sensor transfer function, the parameters that affect sensitivity and linearity, and the effect on frequency response of different sensing film thicknesses and backing configurations have been investigated.

## II. PRINCIPLES OF OPERATION

Fig. 1 shows a schematic of the particular configuration explored in this paper. It comprises a large diameter ( $\sim 1$  cm) Fabry-Perot polymer film sensing element bonded to a transparent backing, immersed in water, and illuminated with a free-space collimated laser beam. A partially reflective aluminium coating on one side of the sensing film and a fully reflective coating on the other side form the mirrors of the interferometer. An incident acoustic wave modulates the optical thickness of the film, producing an optical phase shift  $d\phi$  between the optical fields reflected from the two sides of the film and resulting in a corresponding reflected intensity modulation  $dI_r$  (Fig. 2). For small acoustically induced phase shifts, linear

$$I_r = I \left[ r_{1+}^2 + \frac{(t_{1+}t_{1-}r_2)^2 + 2t_{1+}t_{1-}r_1+r_2 (\cos(\Phi + \tau_{1-} + \tau_{1+} + \beta_2 - \alpha) - r_{1-}r_2 \cos(\tau_{1+} + \tau_{1-} - \beta_1 - \alpha))}{1 + (r_1 - r_2)^2 - 2r_{1-}r_2 \cos(\Phi + \beta_1 + \beta_2)} \right] \quad (1)$$

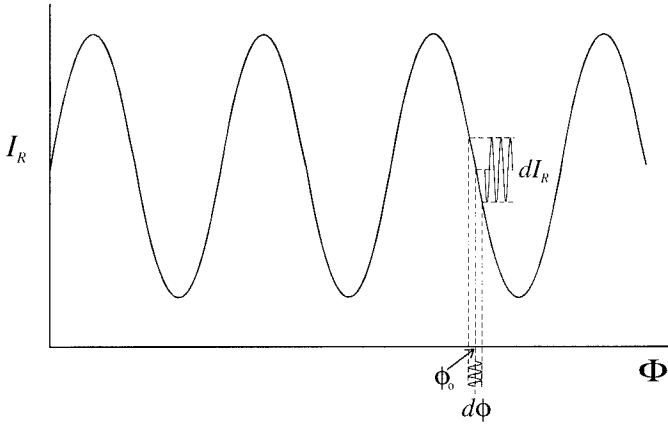


Fig. 2. Interferometer transfer function showing optical output  $I_R$  of interferometer as a function of phase difference  $\Phi$ . Diagram illustrates operation at optimum phase bias  $\phi_0$  for the linear detection of acoustically induced phase modulation  $d\phi$ .

operation can be achieved by tuning the laser wavelength to adjust the initial phase bias  $\phi_0$  so that it lies on the most linear region of the interferometer transfer function (ITF), the so-called active homodyne method. Therefore, the transduction mechanism is one in which the external acoustic pressure produces an optical phase shift that is converted to an intensity modulation via the ITF. This is discussed in the following subsections by way of the ITF, the definition of figures of merit for sensitivity, and a theoretical model of frequency response.

#### A. Interferometer Transfer Function

The relationship between the reflected optical output of the interferometer  $I_r$  and optical phase is termed the ITF. The ITF provides a means of determining and optimizing the measurand-independent optical phase sensitivity of the interferometer and its linear phase range. Additionally, it enables the wavelength tuning requirements of the laser source to be defined.

In its most general form, the ITF for a plane parallel Fabry-Perot cavity, illuminated by a collimated beam of intensity  $I$  is given by (1), where  $r_{1+}$  is the amplitude reflection coefficient for a ray traveling from left to right at the first surface, and  $\alpha$  is the corresponding phase change on reflection at this surface [7], [8]. For a ray traveling in the opposite direction also incident on the first surface, the reflection coefficient is  $r_{1-}$  and the accompanying phase change is  $\beta_1$ ;  $t_{1+}$  is the amplitude transmission coefficient through surface 1 for left-to-right propagation where  $t_{1+}^2 = (1 - r_{1+}^2 - A)$  where  $A$  is the fraction of light absorbed at the first surface. The accompanying phase change on transmission in this direction is  $\tau_{1+}$ . Sim-

ilarly,  $t_{1-}$  is the transmission coefficient, and  $\tau_{1-}$  is the phase change, for propagation in the opposite direction with  $t_{1-}^2 = (1 - r_{1-}^2 - A)$ . These reflection and transmission coefficients and their associated phase changes are not necessarily the same irrespective of propagation direction as they depend upon the refractive indices of the media on either side of the surface. Finally,  $r_2$  is the amplitude reflection coefficient at surface 2, and  $\beta_2$  is the corresponding phase shift upon reflection. Of particular relevance to this study is the low finesse Fabry-Perot ITF which approximates to the raised cosine form of a two beam interferometer. This occurs when the contribution of multiple reflections to the reflected fringe system is negligible; a situation that arises when  $r_{1(+/-)}$  and  $r_2$  are small or when  $A$  is large; the latter is the case with the partially reflective aluminium films [9] used in this study.

When the interferometer is operated as a sensor (Fig. 2), the phase term  $\Phi$  in (1) is made up of a dc phase bias  $\phi_0$  which defines the operating point of the interferometer and the acoustically induced phase shift  $d\phi$  such that

$$\Phi = \phi_0 + d\phi. \quad (2)$$

By setting the phase bias  $\phi_0$  (by adjusting the laser wavelength) so that it lies on the point of maximum slope on the ITF and ensuring that the  $d\phi$  is small, linear operation can be achieved. The linear phase range depends upon finesse; for a low finesse FPI, for example, phase shifts up to 0.5 rad can be resolved with a linearity of better than 5%.

#### B. Sensitivity

When considering sensitivity, it is instructive to define figures of merit that represent the slope efficiency of the conversion of optical phase shift to intensity (phase sensitivity) and the conversion of acoustic pressure to phase shift (acoustic phase sensitivity).

The phase sensitivity  $I_s$  is a measurand-independent term describing the sensitivity of the interferometer to measured-induced phase shifts. It is defined as the optical power modulation per unit phase shift ( $\mu\text{W}/\text{rad}$ ) at the phase bias of the interferometer, thus:

$$I_s = \left[ \frac{dI_r}{d\phi} \right]_{\phi_0}. \quad (3)$$

Therefore,  $I_s$  is dependent upon the incident laser power and the reflectivity and absorbance characteristics of the reflective coatings that form the mirrors of the interferometer. Knowledge of the detector noise floor enables  $I_s$  to be used to determine the phase resolution of the interferometer.

The acoustic phase sensitivity  $A_s$  represents the magnitude of the optical phase shift produced per unit acoustic pressure (rad/MPa). Thus it is a measure of the acoustically induced change in optical thickness of the sensing film, the change in both physical thickness and refractive index.

$$A_s = \frac{d\phi}{dP} = \frac{4\pi nl}{\lambda} \frac{1}{E} \left( 1 + \frac{n^2 p \sigma}{2} \right) |P_I(k)| \quad (4)$$

where  $n$  is the refractive index,  $l$  is the thickness of the film,  $\lambda$  is the laser wavelength,  $E$  is the Young's modulus,  $p$  is the photoelastic constant,  $\sigma$  is Poisson's ratio.  $k$  is the acoustic wavenumber,  $k = 2\pi/\lambda_a$  where  $\lambda_a$  is the acoustic wavelength.  $P_I(k)$  is a frequency-dependent modifying term (discussed further in Section II,C) representing the net stress integrated across the thickness of the sensing film and is dependent upon the acoustic properties of the film, the backing material, and the surrounding media (usually water). In the low frequency limit where  $\lambda_a \gg l$ , assuming the acoustic impedance mismatch between the sensing film and the surrounding fluid is small,  $|P(k)|$  is dominated by the acoustic properties of the backing material. At low frequencies,  $|P(k)| = 0$  for a compliant backing such as air,  $|P(k)| \sim 1$  for a backing of similar acoustic impedance such as water or a polymer and  $|P(k)| \sim 2$  for a rigid backing such as glass [1]. In this paper, the low frequency limit is implied when discussing acoustic phase sensitivity for a particular backing configuration. The acoustic phase sensitivity enables (with knowledge of the form of the ITF) the acoustic pressure range over which the sensor is linear to be estimated and comparisons to be made between the intrinsic sensitivity of different sensing film materials, thicknesses, and backing configurations.

The overall sensitivity  $S$  is the reflected optical power modulation per unit acoustic pressure ( $\mu\text{W}/\text{MPa}$ ). It is the product of  $I_s$  and  $A_s$ :

$$S = \frac{dI_r}{dP} = I_s A_s. \quad (5)$$

Although  $S$  depends upon both  $A_s$  and  $I_s$ , it is the latter that offers the most scope for optimizing sensitivity. This can be achieved by selecting optimal values of  $r_1$  and  $A$  and increasing the incident laser power until the dc interferometer output is close to the saturation threshold of the detector. Even with relatively low reflectivities, this is readily achieved with an incident laser power of a few mW because the saturation threshold of a typical 30 MHz silicon photodiodetransimpedance amplifier configuration is typically less than 100  $\mu\text{W}$ . In principle,  $A_s$  also could be optimized by selecting a polymer film that has the required material properties such as a low Young's modulus. In practice, however, the selection of the polymer film tends to be dominated by considerations such as adequate uniformity of thickness, surface finish, and optical clarity.

### C. Frequency Response

The frequency response is represented by  $P_I(k)$  and is obtained by considering the mean distribution of stress  $P_T$

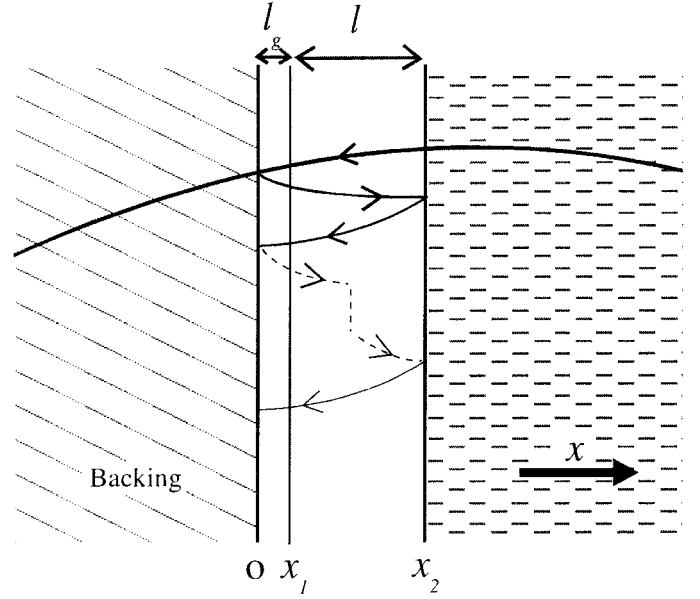


Fig. 3. Geometry used to model frequency response of a sensing film of thickness  $l$  and adhesive layer thickness  $l_g$ .

across the thickness  $l$  of the sensing film due to an incident acoustic wave:

$$P_I(k) = \frac{1}{l} \int_l P_T dx, \quad (6)$$

$P_T$  is the sum of the component of the incident acoustic wave that is transmitted into the sensing film and subsequent acoustic reflections that arise at boundaries at which there are acoustic impedance mismatches. It is assumed that the lateral dimensions of the sensing film are sufficiently large to neglect radial resonance modes and the effects of acoustic diffraction around the edge of the film.

We considered the case shown schematically in Fig. 3, in which a sensing film of thickness  $l$  and infinite lateral dimensions is bonded with an adhesive to a backing material of infinite extent. The thickness of the adhesive layer is  $l_g$ . For a sinusoidally varying incident acoustic wave of unit amplitude and acoustic angular frequency  $\omega$  traveling in the negative  $x$  direction,  $P_T$  is given by:

$$P_T = T \sum_{i=0}^{\infty} \left( (R_0 R_2)^i e^{j(\omega t - k(2x_2 i - x))} + R_0^{i+1} R_2^i e^{j(\omega t - k(2x_2 i + x))} \right) \quad (7)$$

where  $x_1$  and  $x_2$  represent the boundaries of the adhesive layer and the sensing film, respectively, and  $T$  is the pressure amplitude transmission coefficient.  $R_0$  is the pressure amplitude reflection coefficient due to the acoustic impedance mismatch between the adhesive layer and the backing material.  $R_2$  is the pressure amplitude reflection coefficient at the boundary between the sensing film and the surrounding medium (usually water). It is assumed that the acoustic impedance of the sensing film and the

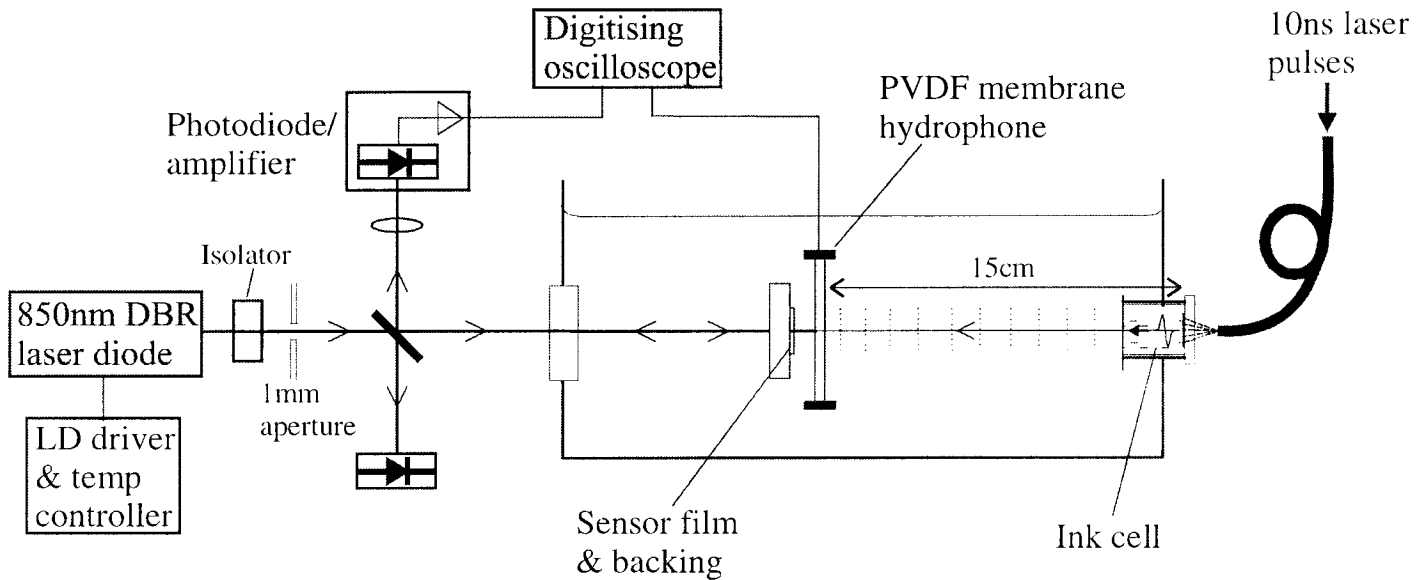


Fig. 4. Schematic of experimental set-up.

adhesive layer (see Section III for experimental validation of this assumption) are the same. Thus there are no reflections at the boundary between the two. Acoustic attenuation in the film and the adhesive layer also is assumed to be negligible. Evaluating (7) as the sum of an infinite series yields

$$P_T = T \left( \frac{1}{1 - R_0 R_2 e^{-2jkx_2}} \right) e^{j\omega t} (e^{jkx} + R_0 e^{-jkx}). \quad (8)$$

From (6):

$$P_I(k) = \frac{T}{l} \left( \frac{1}{1 - R_0 R_2 e^{-2jkx_2}} \right) e^{j\omega t} \int_{x_1}^{x_2} (e^{jkx} + R_0 e^{-jkx}) dx. \quad (9)$$

Evaluating the integral in (9), taking the complex conjugate and making the substitutions  $x_1 = l_g$  and  $x_2 = l + l_g$  gives (10) (top of next page).

### III. EXPERIMENTAL SET UP AND METHOD

The experimental set-up shown in Fig. 4 was used to obtain the ITF and determine the sensitivity and frequency response for a range of sensor configurations.

The polymer film sensing elements comprised 1 cm diameter sections of 23- $\mu\text{m}$  or 50- $\mu\text{m}$  thick PET with a 20% reflective aluminium coating ( $A \sim 35\%$ ) deposited onto one side of the film and a 75% reflective coating on the other side. These sensing elements were bonded to transparent 3-mm thick polymethylmethacrylate (PMMA) or 5-mm thick glass backing stubs using a UV curable optical

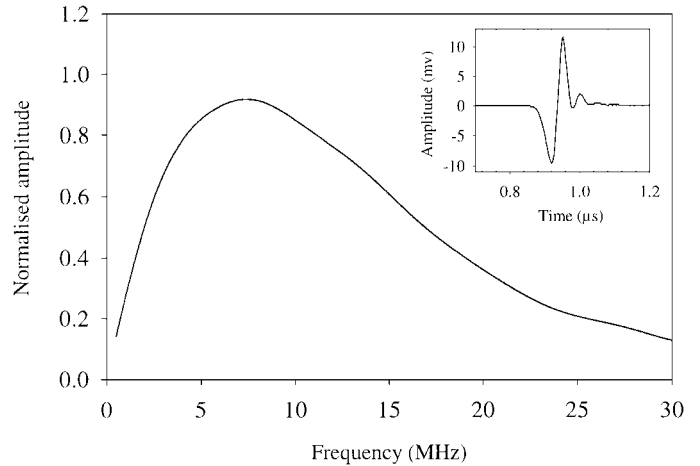


Fig. 5. Corrected frequency spectrum of acoustic pulse (inset) measured by the PVDF membrane hydrophone at a distance of 15 cm from source.

adhesive (Norland NOA 68). Pressure was applied during the curing process to minimize the thickness of the adhesive layer. The density of the adhesive was 1260 Kg/m<sup>3</sup> and the speed of sound was measured to be 2400 m/s, giving an acoustic impedance of  $3 \times 10^6$  Kg/m<sup>2</sup>s, close to that of PET ( $3.1 \times 10^6$  Kg/m<sup>2</sup>s).

The sensor film-backing stub was illuminated with the collimated output of an 850 nm Distributed Bragg Reflector (DBR) laser diode. The light reflected from the sensing film was directed via a beamsplitter onto a 25 MHz pin photodiode-amplifier unit of known sensitivity and frequency response. A second photodiode was used to monitor the output of the laser diode. To adjust the phase bias of the interferometer, the wavelength of the laser diode was thermally tuned by adjusting the current supplied to the internal Peltier element within the laser diode package. The maximum tuning range was approximately 4 nm.

$$|P_l(k)| = \frac{T\sqrt{2}}{kl} \sqrt{\frac{(R_0^2 + 1) + 4R_0 \cos k(l + 2l_g) \sin^2(kl/2) - (1 + R_0^2) \cos kl}{1 - 2R_0R_2 \cos 2k(l + l_g) + (R_0R_2)^2}}. \quad (10)$$

The acoustic performance was evaluated by comparing the sensor response to a broadband pulsed acoustic field with that of a calibrated 50  $\mu\text{m}$  bilaminar PVDF membrane hydrophone (Marconi Y-33-7611) of 1 mm active diameter and of known sensitivity and frequency response. The acoustic source consisted of an ink cell onto which 10 ns laser pulses at 532 nm were incident. The laser pulses were delivered using a 10 m length of 400  $\mu\text{m}$  core multi-mode optical fiber. The beam diameter on the ink cell was 4 mm. To ensure that the incident illumination was uniform, the fiber was tightly coiled in order to excite all the propagation modes equally. Absorption of the laser pulses in the ink results in rapid thermoelastic expansion leading to the generation of short ( $\sim 150$  ns) bipolar pulses of ultrasound (peak positive acoustic pressure  $\sim 0.07$  MPa) that propagate away from the illuminated region. A typical frequency spectrum of the acoustic signal measured by the membrane hydrophone at a distance of 15 cm from the ink cell is shown in Fig. 5. A correction was applied to the spectrum shown in Fig. 5 to take into account the frequency response characteristics of the hydrophone. For accurate measurement of the sensor frequency response and sensitivity, it is important that the active region of the sensing film (defined by the dimensions and position of the illuminating laser beam) is in the same lateral and axial point in the acoustic field as the membrane hydrophone. Even more importantly, given the high directivity of the membrane hydrophone [10] at MHz frequencies due to its relatively large active diameter (1 mm), the dimensions of the active regions of the sensor and hydrophone and the angle they present to the incident acoustic field should be identical. The optical nature of the sensor is an advantage in these respects because the laser beam can be easily apertured to match the 1 mm active diameter of the membrane hydrophone. Ensuring that the angle of the incident acoustic field is the same for both devices was achieved by adjusting the angle of incidence of the laser beam using beamsteering mirrors (not shown in Fig. 4) so that it was normally incident on the active region of the membrane hydrophone. The specular reflection from the gold coated surface of the hydrophone was then “followed” back to the photodiode, the position of which was adjusted to give maximum output. After taking a measurement, the membrane hydrophone was removed and replaced by the sensing film. By adjusting the axial position and angle of the sensing film alone (the beamsteering mirrors and the photodiode position were not touched) so that the photodiode output was again at a maximum, it could be ensured that the sensing film was aligned at the same angle as the membrane hydrophone.

## IV. RESULTS

### A. Interferometer Transfer Function

To obtain the interferometer transfer function, a 50  $\mu\text{m}$  thick PET sensing film was used. No backing stub was employed; thus, in this configuration water is in contact with both sides of the sensing film. Fig. 6 shows the experimentally measured ITF obtained by thermally tuning the laser diode over a range of approximately 3.5 nm and monitoring the output of the photodiode. A correction was applied to take into account the variation in laser diode output power with operating temperature. The raised sinusoidal shape of the fringe shown in Fig. 6 indicates low finesse operation, although in the absence of a complete fringe (due to the limited tuning range of the laser), some caution must be exercised in relating fringe shape to finesse due to the asymmetric nature of reflected fringes that can occur with metal films [8]. Given the strong optical absorption ( $A \sim 0.35$ ) of the partially reflective aluminium coating [9] on the front surface of the sensing film, however, it is reasonable to assume that the interferometer is indeed of low finesse. Thus the horizontal axis of Fig. 6 can be calibrated in radians of optical phase by assuming there are  $\pi$  radians of phase shift between a maximum and a minimum of the ITF. By converting from intensity to phase, as discussed later, the acoustic phase sensitivity and linear operating range of the sensor can be determined.

### B. Sensitivity

To determine acoustic phase sensitivity, the water-backed 50- $\mu\text{m}$  thick PET film, for which the ITF in Fig. 6 is shown, was used. In this configuration,  $|P(k)| = 1$  for  $\lambda_a \gg l$  as is the case for the configuration in which there are no acoustic impedance mismatches on either side of the film [1]. The water backed configuration, therefore, provides a convenient and practical benchmark configuration for comparison purposes. With the laser wavelength adjusted so that the phase bias was set halfway between the ITF maximum and minimum, the so-called quadrature point, the intensity modulation produced by an acoustic signal of known amplitude was converted, using Fig. 6, to the corresponding phase modulation giving  $A_s = 0.1$  rad/MPa. It is not possible to identify the relative contributions of the acoustically induced changes in thickness and refractive index to the net optical phase shift due to the paucity of data available on the typical values of  $E$ ,  $\sigma$ , and  $p$  at ultrasonic frequencies for PET.

The phase resolution of the interferometer was found to be 2 mrad over a 25 MHz measurement bandwidth (without signal averaging) by dividing the noise-equivalent

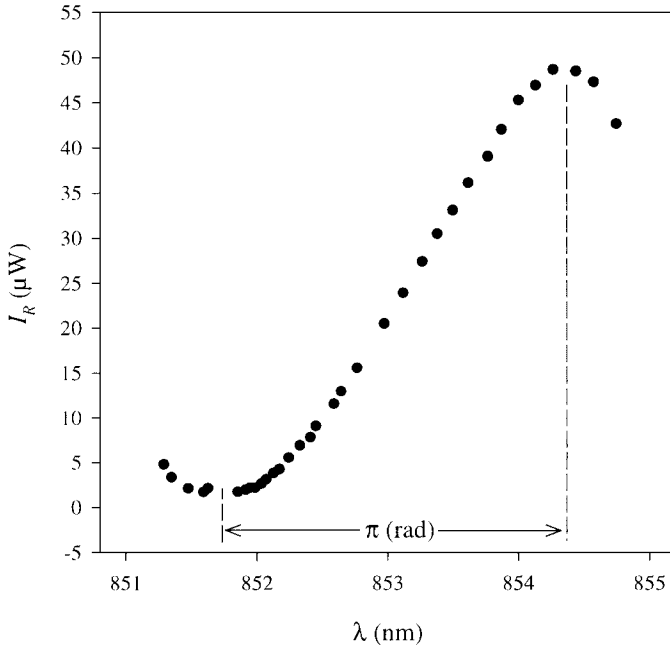


Fig. 6. Interferometer transfer function of a 50  $\mu\text{m}$  PET sensing film obtained by tuning the laser wavelength  $\lambda$ .

power of the detector unit (0.04  $\mu\text{W}$ ) by  $I_s$  (21  $\mu\text{W}/\text{rad}$ ). The corresponding noise-equivalent pressure (from  $A_s$ ) is, therefore, 20 kPa. Improved sensitivity could be obtained by increasing the incident laser power to just below the detector saturation threshold to obtain the 10 kPa resolutions previously reported [3].

### C. Linearity

For a low finesse interferometer operating at quadrature, phase shifts of up to around 0.5 rad can be detected with a linearity of better than 5%. With  $A_s = 0.1$  rad/MPa this indicates that the linear range of a water-backed 50- $\mu\text{m}$  thick PET film extends to approximately 5 MPa.

### D. Frequency Response

The effect on frequency response of different sensing film thicknesses, backing materials, and the adhesive layer thickness was studied. The frequency response was obtained by comparing the discrete Fourier transforms of the time domain waveforms detected by the sensor and the membrane hydrophone. Appropriate corrections were applied to take into account both the frequency response characteristics of the photodiode and the membrane hydrophone.

The results in Fig. 7 show a comparison between the measured normalized frequency response and that obtained using (10) (with  $l_g = 0$ ) for 50  $\mu\text{m}$  and 23  $\mu\text{m}$  PET sensing films in water-backed, glass-backed, and PMMA-backed configurations.

The measured response in Fig. 7(a) is in good agreement with the predicted response demonstrating the  $\lambda/2$  thickness mode resonance at 20 MHz characteristic of a water-

backed polymer film. The PMMA backed configurations in Figs. 7(c) and (f) also compare well with theory. In this configuration, the adhesive layer has a very similar acoustic impedance to both the sensing film and the backing material and, therefore, does not significantly influence the frequency response characteristics. Where there are discrepancies, they tend to appear at the higher frequencies (>20 MHz) at which uncertainties due to low signal-noise ratio, timing jitter, spatial field variations, and differences in angular alignment between the sensor and hydrophone have the greatest influence.

Departures from the model are more apparent in the glass-backed configurations (Fig. 7b and e) at which the finite thickness  $l_g$  of the adhesive layer has a significant influence on frequency response, the most obvious being a reduction in bandwidth. To obtain a value for  $l_g$ , (10) was fitted to the data in Fig. 7(b) and (e) giving  $l_g = 1.6$   $\mu\text{m}$  for both the glass-backed 50  $\mu\text{m}$  and 23  $\mu\text{m}$  films.

The influence of  $l_g$  can be seen more clearly in Fig. 8. Curve A is that of Fig. 7(b) in which the sensing film was bonded to the glass backing under pressure, thus  $l_g = 1.6$   $\mu\text{m}$ . Curve B shows the response obtained using a 23  $\mu\text{m}$  spacer between the PET film and the backing. Fitting (10) gives a value of  $l_g = 21$   $\mu\text{m}$ , indicating that the model provides an accurate indication of adhesive layer thickness. Curve C was obtained by bonding the sensing film without applying pressure. Fitting (10) to curve C gives  $l_g = 80$   $\mu\text{m}$ . For all three curves, agreement between the shape of the experimental and fitted frequency response is excellent.

As expected, the adhesive layer is detrimental to performance, resulting in a reduced bandwidth and the introduction of features beyond the  $\lambda/2$  minimum. These effects are noticeable even for very small  $l_g$ . As  $l_g$  becomes comparable to  $l$ , the bandwidth is significantly reduced and large variations in sensitivity appear. If bandwidth is not to be compromised, it is desirable to limit the adhesive layer thickness to only a few microns for sensing films of a few tens of  $\mu\text{m}$  thick.

### E. Water Absorption

Water absorption changes the thickness of the sensing film by swelling. If large enough this can cause changes in sensitivity as the phase bias of the interferometer is shifted from its optimum point. The magnitude of this shift was determined by measuring the ITF 0.5, 3.5, and 24 hours after the sensing film was immersed in water. The shift, which had stabilized after 3.5 hours was found to be approximately 1/8 of a fringe (0.8 rad) corresponding to a thickness change of about 30 nm. This is usually of limited significance, but if necessary it could be compensated for by tuning the laser diode wavelength.

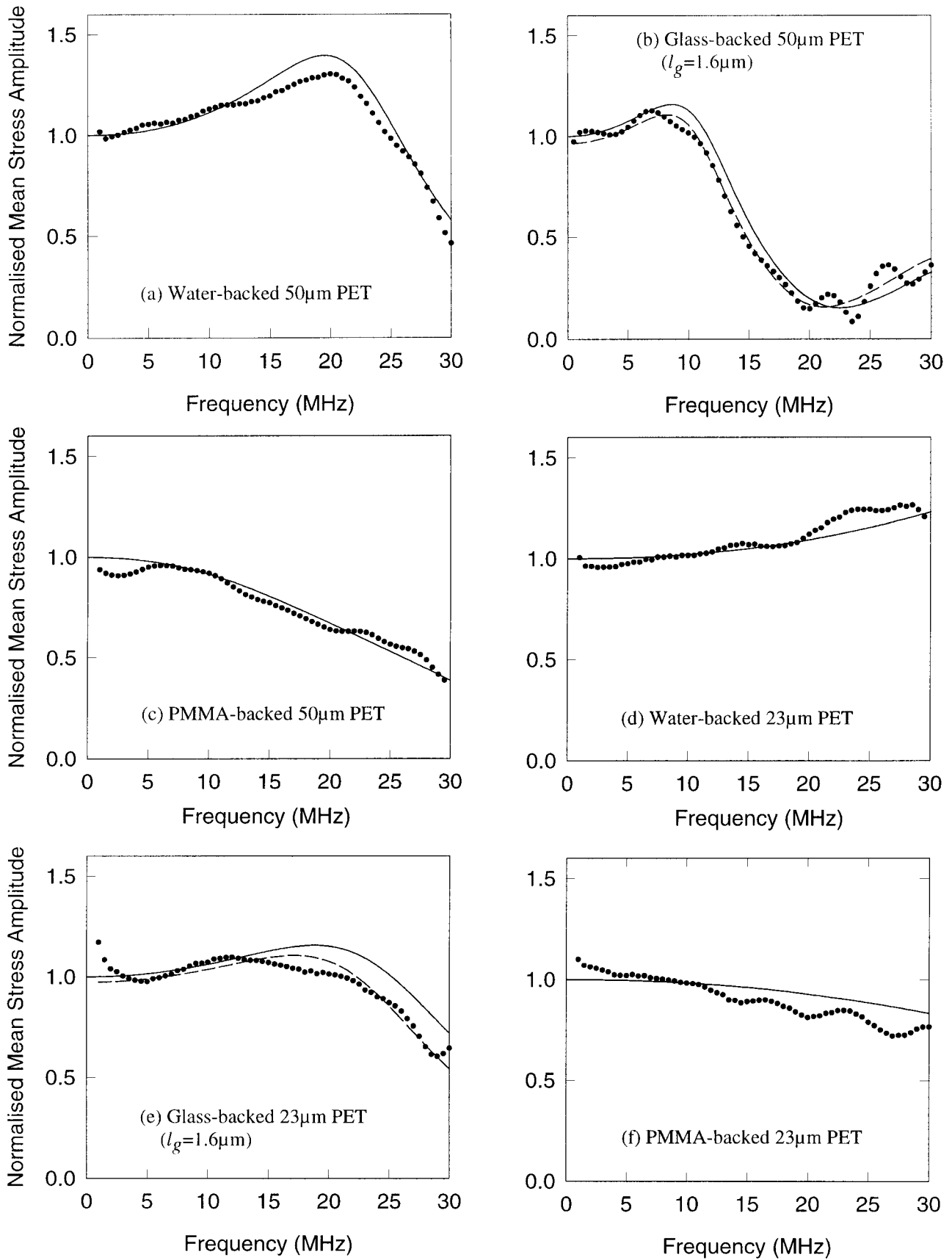


Fig. 7. Normalized frequency response for different sensing film thicknesses and backing configurations. • experimentally measured response, — predicted response with  $l_g = 0$ , and ---- fit of equation 10 to experimental response.

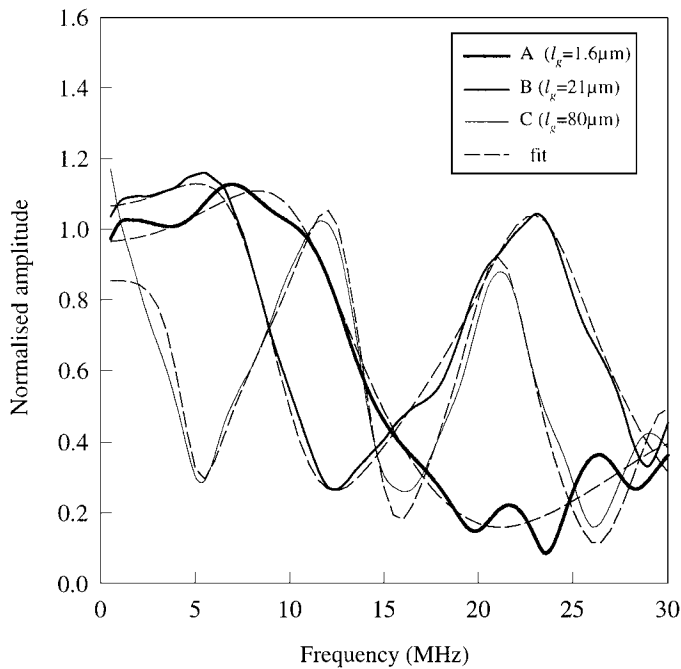


Fig. 8. Effect of adhesive layer thickness  $l_g$  on the frequency response of a  $50 \mu\text{m}$ -thick, glass-backed PET sensing film. The solid lines represent the experimentally measured responses. The dashed lines show the fit to the data using (10). The values of  $l_g$  given in the legend are those obtained from the fit to the data.

## V. CONCLUSION

Aspects of the transduction mechanisms of the Fabry-Perot polymer film ultrasound sensor have been investigated. Comparisons between the frequency response model and experimental data show that, in a rigid-backed configuration, the adhesive layer should be no more than a few microns thick to avoid significantly degrading the frequency response. This may have implications for the fabrication of probe-type configurations [2], [4], [5], in which discrete sensing elements are bonded to the tip of an optical fiber, as the small dimensions involved are likely to make it difficult to achieve such small adhesive layer thicknesses.

The technique for converting acoustic pressure at ultrasonic frequencies to the corresponding optical phase shift via the ITF provides a broadly applicable means of eliciting information about the operation of the sensor to further its understanding and for optimization and characterization purposes. For example, it enables the overall

measured sensitivity to be interpreted in terms of the relative contributions of phase sensitivity and acoustic phase sensitivity enabling direct comparisons between different sensing configurations to be made.

This study has shown that this type of sensor can detect ultrasound to 30 MHz with a sensitivity of 10 kPa over a 25 MHz measurement bandwidth. This is comparable to the performance of piezoelectric PVDF film transducers. An important advantage, however, is that the dimensions of the active area, which are defined by the illuminating beam diameter, can, in principle, be reduced to the optical diffraction limit of a few  $\mu\text{m}$  without compromising sensitivity. This offers the prospect of fabricating very small aperture, wideband ultrasound receivers that overcome the sensitivity limitations of small element piezoelectric transducers.

The favorable acoustic performance, design flexibility, and simplicity of operation suggest that this type of transducer has the potential to provide a realistic alternative to wideband piezoelectric ultrasound detection technology for field measurement and imaging applications.

## REFERENCES

- [1] P. C. Beard and T. N. Mills, "Extrinsic optical fibre ultrasound sensor using a thin polymer film as a low finesse Fabry-Perot interferometer," *Appl. Opt.*, vol. 35, no. 4, pp. 663-675, 1996.
- [2] —, "A miniature optical fibre ultrasonic hydrophone using a Fabry-Perot polymer film interferometer," *Electron. Lett.*, vol. 33, no. 9, pp. 801-803, 1997.
- [3] P. C. Beard, A. Hurrell, E. van den Elzen, and T. N. Mills, "Comparison of a miniature ultrasonic optical fibre hydrophone with PVDF hydrophone technology," *Proc. IEEE Ultrason. Symp.*, 1998, pp. 1881-1884.
- [4] A. J. Coleman, E. Draguioti, R. Tiptaf, N. Shetri, J. E. Saunders, "Acoustic performance and clinical use of a fibreoptic hydrophone," *Ultrason. Med. Biol.*, vol. 24, no. 1, pp. 143-151, 1998.
- [5] P. C. Beard, F. Perennes, E. Draguioti, T. N. Mills, "An optical fibre photoacoustic-photothermal probe," *Opt. Lett.*, vol. 23, no. 15, pp. 1235-1237, 1998.
- [6] F. Pérennès, P. C. Beard, T. N. Mills, "Analysis of a low finesse Fabry Perot sensing interferometer illuminated by a multimode optical fiber," *Appl. Optics*, vol. 38, no. 34, Dec. 1999.
- [7] J. M. Vaughan, *The Fabry-Perot Interferometer—History, Theory, Practice and Applications*, (Adam Hilger Series on Optics and Optoelectronics). Bristol: IOP Publishing, 1989, p. 94.
- [8] J. Holden, "Multiple beam interferometry: Intensity distribution in the reflected system," *Proc. Phys. Soc. Section B*, vol. 62, part 7, no. 355B, pp. 405-417, 1949.
- [9] L. Holland, *Vacuum Deposition of Thin Films*, London: Chapman & Hall, 1970.
- [10] D. R. Bacon, "Characteristics of a pvdf membrane hydrophone for use in the range 1-100 MHz," *IEEE Trans. Ultrason., Ferroelect., Freq. Contr.*, vol. SU-29, no. 1, pp. 18-25, 1982.